

Formation of photoelectron spectra of alloys niobium-molybdenum-zirconium

Yokub Ergashov^{1*}, Burkhon Donaev², Sherzod Khudainazarov³, and Jakhongir Normuminov¹

¹Tashkent State Technical University after I.Karimov, Tashkent, Uzbekistan

²Karshi engineering-economical institute, Karshi, Uzbekistan

³Tashkent Institute of Irrigation and Agricultural Mechanization Engineers, Tashkent, Uzbekistan

Abstract. Crystals of niobium and its alloys obtained by low-energy implantation of molybdenum and zirconium ions were studied in a multi-functional installation. The energy distribution curves of N (E) photoelectrons before and after heating niobium – molybdenum – zirconium alloys were studied. The contribution of surface zones formed by molybdenum and zirconium atoms to photoelectron emission in the photon energy region of 8–10 eV was analyzed.

1 Introduction

Recently, as it is known, one of the most urgent tasks of physical electronics and nanotechnology is the creation of surface alloys of arbitrary composition with the necessary concentration of alloying elements. Alloys of refractory metals based on niobium, molybdenum, tantalum, and others are widely used in nuclear power, mechanical engineering, vacuum technology, etc. Experimental and theoretical studies of several alloys have shown that controlling the state of s-d electrons by introducing small concentrations of alloying elements and creating surface alloys allows us to solve some fundamental problems of an applied and theoretical nature. Alloys obtained by traditional methods have their drawbacks. One of the disadvantages of such alloys is the difficulty of obtaining atomically pure systems with a low content of carbon, oxygen, and sulfur atoms. The production of alloys by implanting ions of various refractory metals under ultrahigh vacuum conditions can eliminate this specified disadvantage. In this paper, using the example of implantation of low-energy Mo and Zr ions in a single crystal Nb (110), we study the change in the spectral dependence of the quantum photoemission yield (QPhY). The value of the photoemission work of the output is found, and the features of the formation of photoelectron spectra of N(E) in the near and vacuum ultraviolet are studied [1-8].

* Corresponding author: yergashev@mail.ru

2 Materials and methods

The design of a multi-functional ultra-high-vacuum experimental setup with a solid-state ion source is described in [9-13]. Crystals of Nb, Mo, and Zr, placed in a tantalum cup, were heated to a temperature of 2000-2200 K to clean the surface from impurity elements. The working vacuum in the device chamber was $(3-5) \times 10^{-10}$ Torr. During the implantation of Mo and Zr ions, the residual gas pressure in the unit was no higher than $(2-3) \times 10^{-8}$ Torr. The flow of Mo and Zr ions in this mode is equal to $\sim 10^{11}$ ion·sm⁻²·s⁻¹, and the ion energy $E = 3-3.5$ keV.

Monocrystals Mo(111), Nb(110), and polycrystalline zirconium were mounted in the manipulator of the experimental setup. The crystals were preheated to $T = 2200-2400$ K for more than 50 hours. The cleanliness of the surface was monitored by Auger spectra. The Auger spectra of the samples were measured in the energy range from 80 to 600 eV after high-temperature heating, as well as in heated crystals. The spectral dependences of the QPhY were removed, and the value of the work function was determined by the method of straight and isothermal Fowler's curves. In this case, graphs of the dependence in the photon energy range from 3.95 to 5.15 eV were plotted. The sample temperature was maintained at room temperature when removing the QPhY. The photoelectrons' energy distribution curves were obtained at photon energies $h\nu = 8.4$ and 10 eV, and xenon and krypton resonance lamps were used as radiation sources.

3 Results and discussion

After thermal cleaning of the samples under study, the Auger spectra of the surface of Nb, Mo, and Zr single crystals were taken. Figure 1 shows the Auger spectra after implantation of Mo and Zr ions in Nb (110), where the main peaks of niobium, the peaks of molybdenum and zirconium, and a small peak of carbon are visible. Figure 1 shows the Auger spectra after implantation of Mo and Zr ions in Nb (110), where the main peaks of niobium, the peaks of molybdenum and zirconium, and a small peak of carbon are visible. The maximum surface concentration of the implanted molybdenum and zirconium atoms is reached after heating the sample to 1350-1400 K. Further heating of the crystal (over 1400 K) leads to a decrease in the surface concentration of molybdenum and zirconium. To find the distribution of Mo and Zr atoms in-depth in Nb(110), the crystal surface was etched layer-by-layer with argon ions. At the current density and ion energy used, $E_p = 1$ keV, one layer of Mo and Zr atoms was removed in $\sim 6-7$ min. After removing $\sim 8-10$ atomic layers from the crystal surface, the concentration of Mo and Zr atoms decreased to ~ 1 at. %.

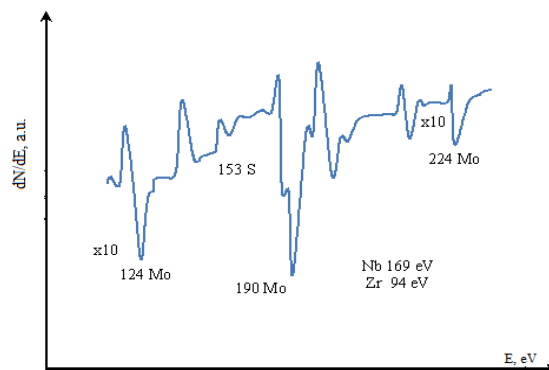


Fig.1. Auger spectra of the diluted Nb-Mo-Zr alloy, after heating $T=1600-1700$ K.

Quantitative calculations were carried out by the method of the element sensitivity factor. Under the same surface treatment conditions, the spectral dependences of the QPhY of crystals studied before and after implantation of the Nb(110) surface with zirconium ions were removed, and the values of the photoemission work of the output were calculated. If before implantation for Nb (110) $\varphi = 4.52 \pm 0.02$ eV, then after implantation, this value was equal to $\varphi = 4.38-4.40$ eV, i.e., there is a decrease in the output operation by ~ 0.15 eV. To facilitate the interpretation of the obtained $N(E)$ photoelectron spectra for the Nb-Mo-Zr alloy, the energy distribution curves of the photoelectrons were taken from the Mo(110) surface and the atomically pure surface of zirconium. Figure 2 shows the $N(E)$ of an atomically pure Mo (111) crystal. It can be seen that in the spectra of photoelectrons taken from the surface of Mo (111) at a photon energy of 8.4 eV, there are three maxima at energy values of 0.5, 1.4, 2.4 eV (curve 1), and at 10 eV there are two more maxima – 3.8 and 4.5 eV (curve 2) below the Fermi level. The position of peaks A and B with energies of -0.5 eV and -1.4 eV below the Fermi level is independent of the photon energy. Peak B is shifted by 0.2 eV on the energy scale (curves 1, 2).

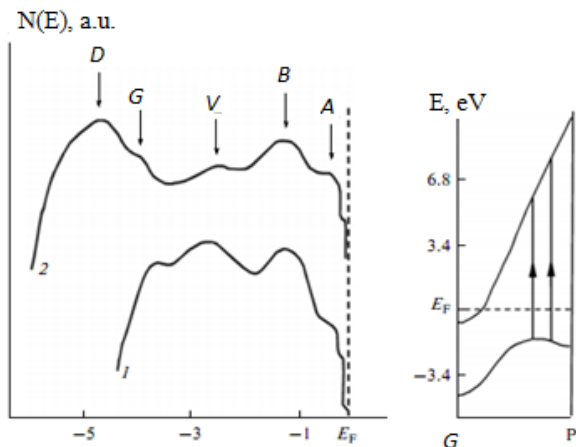


Fig.2. Photoelectron spectra of a pure Mo (111) monocrystal and a region of the band structure in the direction of symmetry of the GR: 1-at the photon energy of 8.4 and 2- at the energy of 10 eV

Figure 3 shows the photoelectron spectra for an implanted Nb (110) crystal by Mo and Zr ions, recorded at $h\nu = 8.4$ eV. After heating at $T = 1200$ K (curve 1) and $T = 1400$ K (curve 2), a number of features are observed in the regions of 0.5 eV, 1.3 eV, 1.4–1.5 eV, and 2.1–2.2 eV below the Fermi level. In contrast to pure niobium, the $N(E)$ curve had a broad maximum in the low-energy region, and after heating at $T = 1400$ K, a decrease in the intensity of this maximum was observed. The same figure shows the photoelectron spectrum for a pure Mo (111) single crystal (curve 1). Comparing these three curves, we can say the following. The C peak at 1.2–1.3 eV is most likely associated with the density of electronic states of hafnium since the position of this maximum did not change after the photoelectron spectra were taken at $h\nu = 10$ eV. We associate peaks A and C with indirect optical transitions [13,14] for a pure Mo (111) single crystal. Thus, the photoelectron spectra for pure Mo (111) exhibit maxima due to the band structure of molybdenum, and in

the spectrum obtained after doping with zirconium ions, an additional maximum appears at 1.2-1.3 eV below the Fermi level [15-20].

It is shown in [10] that when low-energy ions of refractory metals are implanted, the alloying atoms are mainly distributed in the near-surface region of the metal matrix with a depth of up to ten atomic layers. Suppose before implantation of the Mo(111) KVF sample there is a significant increase in the quantum yield of the photoemission as a function of the energy of the incident photons, then after implantation. In that case, there is a weak dependence $Y = f(h\nu)$. This is probably due to a violation of the order of the structure of the surface atomic layer and a change in the surface reflection coefficient after the implantation of hafnium atoms. Secondly, the introduced ions form a solid substitution solution with the matrix, which leads to a change in the lattice structure. Photoelectrons involved in the emission from the surface layer lose part of their energy due to the formation of defects and radiation damage during ion insertion. It should also be noted that these processes are affected by the heating of the crystal and the presence of residual gases in the installation. The features of the electronic states of the surface layer of the alloy are clearly shown on the energy distribution curves taken at $h\nu = 8.4$ eV after heating at $T = 1400$ K.

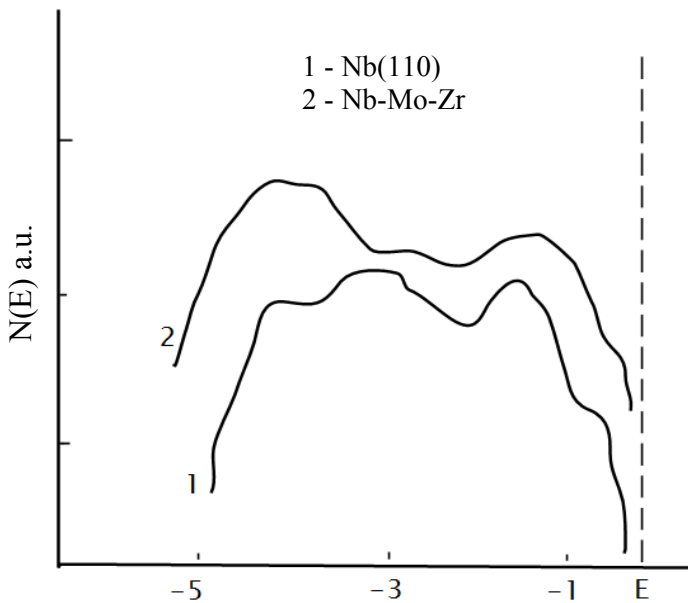


Fig. 3. Photoelectronic spectra of pure (1) and ion-implanted monocrystal of Nb (110); 2-implanted crystal after heating at temperatures of 1400-1500 K.

The origin of the low-energy maximum in pure metals is mainly due to photoelectron's loss of energy during electron-electron inelastic scattering [11]. During ion doping, a cascade of collisions develops in a solid. In this case, many defects such as vacancies and interstitial atoms are formed in the matrix metal. Thus, a significant increase in the amplitude of the low-energy maximum is due to the energy losses of photoelectrons on structural and point defects. The decrease in the amplitude is associated with some ordering of the structure after heating the crystal. Directed photoelectron emission from the surface of niobium (110) was investigated. Our data for the pure Nb(110) surface are in good agreement with the results [21-25]. The position of peaks A and B with energies 0.5 and 1.4

eV below the Fermi level is independent of the photon energy. Such features for the $N(E)$ curves in the indirect transition model [10] correspond to the maxima of the density of the electronic states of the valence band. It should be noted that the peak located directly near the Fermi level (~ 0.5 eV) is very sensitive to surface contamination by adsorbed gases.

4 Conclusion

Apparently, this peak is associated with the surface resonance level. Analysis of the $N(E)$ curves taken at photon energies of 10 and 8.4 eV from the surface of ion-doped niobium shows that additional maxima at energies of 1.25–1.3 eV below the Fermi level are due to implanted molybdenum and zirconium atoms [14]. Implanted niobium atoms create their own energy sub-bands associated with zirconium d-electrons [15]. Apparently, these electronic subbands are located in the forbidden zone in the direction of the symmetry ΓN band structure of niobium [26, 27]. Analyzing the results obtained, we note that the model calculations of the electron output from the bulk and surface states carried out by several authors [9, 25-29] showed that the contribution of the surface states is carried out from ~ 2.5 atomic layers.

References

1. Umirzakov B.E., Donaev S.B. *On the creation of ordered nuclei by ion bombardment for obtaining nanoscale Si structures on the surface of CaF_2 films*, Journal of Surface Investigation, **11**, (4), pp. 746–748. <https://doi.org/10.1134/S1027451017040139>. (2017).
2. Donaev S.B., Tashatov A.K., Umirzakov B.E. *Effect of Ar^+ -ion bombardment on the composition and structure of the surface of $CoSi_2/Si(111)$ nanofilms*. Journal of Surface Investigation, **9**, (2), pp. 406–409. <https://doi.org/10.1134/S1027451015020263>. (2015).
3. Isakhanov Z.A., Umirzakov Y.E., Ruzibaeva M.K., Donaev S.B. *Effect of the O_2^+ -ion bombardment on the TiN composition and structure*., Technical Physics, **60**, No (2), pp. 313–315. <https://doi.org/10.1134/S1063784215020097>. (2015).
4. Umirzakov B.E., Tashmukhamedova D.A., Ruzibaeva M.K., Djurabekova F.G., Danaev S.B. *Investigation of change of the composition and structure of the CaF_2/Si films surface at the low-energy bombardment*. Nuclear Instruments and Methods in Physics Research, Section B: Beam Interactions with Materials and Atoms, (326), pp. 322–325. (2014).
5. Umirzakov B.E., Tashmukhamedova D.A., Ruzibaeva M.K., Donaev S.B., Mavlyanov B.B. *Analysis of the structure and properties of heterostructured nanofilms prepared by epitaxy and ion implantation methods*., Technical Physics, 2013, Vol. 58, No 9, pp. 1383–1386. <https://doi.org/10.1134/S1063784213090260>.
6. Rysbaev A.S., Khuzhaniyazov Z.B., Rakhimov A.M., Bekpulatov I.R. *Formation of nanosize silicides films on the $Si(111)$ and $Si(100)$ surfaces by low-energy ion implantation*, Technical Physics, **59**, (10), pp. 1526–1530. DOI:10.1134/S1063784214100272. (2014).
7. Risbaev A.S., Khujaniyazov J.B., Bekpulatov I.R., Rakhimov A.M. *Method for additional purification of the surface of $Si(111)$ single crystal*, Journal of Surface Investigation, **11**, (5), pp. 994–999. DOI:10.1134/S1027451017050135. (2017).

8. Umirzakov B.E., Ashurov R.K., Donaev S.B. *The Morphology and Electronic Properties of Si Nanoscale Structures on a CaF₂ Surface*. Technical Physics, **64**,(2), pp. 232–235. DOI:10.1134/S1063784219020269.(2019).
9. Buribayev I., Nurmatov N.A., Xolov A. Poverxnost. Rentgen., sinx. i neytron. issled. (8). p. 53. (2004).
10. Ergashov, Y.S., Tashmukhamedova, D.A., Djurabekova, F.G., Umirzakov, B.E. Bulletin of the Russian Academy of Sciences: Physics, **80** (2), **ctp.** 138–140. (2016).
11. Malinenko, V.P., Pergament, A.L., Gorbakov, A.O. Uch. Zap. Petrozav. Univ., Fiz.-Mat. Nauki., **2**, p. 100. (2014)
12. Ergashov, Y.S. Technical Physics, 2017, 62(5), P. 777–780
13. Bugerko, L.N., Borisova, N.V., Surovaya, V.E., Eremeeva, G.O. Polzunov. Vestn., (1), p. 77. (2013)
14. Andreev, V.N., Nikitin, S.E., Klimov, V.A., Kozyrev, S.V., Leshchev, D.V., Shtel'makh, K.F. 2001 Physics of the Solid State, **43** (4), pp. 788-791.
15. Domashevskaya E.P., Terexov V.A. i dr. *FTT*, **55**. (3). p. 577.(2013)
16. Belyayev A.P., Rubets V.P., Antipov V.V., Yeremina Y.O. *FTP*, 2010. T.44. S. 978.
17. Muzafarova S.A., Mirsagatov Sh.A., Janabergenov J. *FTT*. (49). p. 1111. (2007).
18. Yao, J.N., Yang, Y.A., Loo, B.H. Journal of Physical Chemistry B, **102** (11), pp. 1856-1860. (1998).
19. Yokub, E., Boltakhodja, U. E3S Web of Conferences, 178, 01079. (2020).
20. Surovoi, E.P., Borisova, N.V., Bugerko, L.N., Surovaya, V.E., Ramazanov, G.O. Russian Journal of Physical Chemistry A, **87** (12), pp. 2063. (2013).
21. Xie, R., Bui, C.T., Varghese, B., Zhang, Q., Sow, C.H., Li, B., Thong, J.T.L. Advanced Functional Materials, (9), pp. 1602-1607.(2011).
22. Kovivchak V.S., Panova T.V. Journal of Surface Investigation, **10** (6), pp. 1226-1230. (2016).
23. Tong M., Dai G., Wu Y., He X., Gao D. Journal of Materials Science, **36** (10), pp. 2535-2538,(2001).
24. Driscoll T., Kim H.T., Chae B.G., Di Ventra M., Basov D.N. Applied Physics Letters, **95** (4).(2009).
25. Herndon M.K., Gupta A., Kaydanov V.I., Collins R.T. Appl. Phys. Lett. (75). p. 3503. (19990).
26. Ergashov Y.S., Tashmukhamedova D.A., Umirzakov B.E. Journal of Surface Investigation, **11** (2), p. 480–484. (2017).
27. Ergashov, Y.S., Umirzakov, B.E. Technical Physics, **63** (12), p. 1820–1823. (2018).
28. Umirzakov B.E., Tashmukhamedova D.A., Tursunov M.A., Ergashov Y.S., Allayarova G.K. Technical Physics, **64** (7), **ctp.** 1051–1054. (2019).
29. Ergashov E.S., Isakhanov Z.A., Umirzakov B.E. Technical Physics, **61** (6), **ctp.** 953–955. (2016).